MAGNETORHEOLOGICAL LANDING GEAR.

PART 2: VALIDATION USING EXPERIMENTAL DATA

D C Batterbee, N D Sims*, R Stanway, and M Rennison

Department of Mechanical Engineering, The University of Sheffield,
Sheffield, S1 3JD, UK.

ABSTRACT

Aircraft landing gears are subjected to a wide range of excitation conditions with conflicting damping requirements. A novel solution to this problem is to implement semi-active damping using magnetorheological (MR) fluids. In Part 1 of this contribution, a methodology was developed that enables the geometry of a flow mode MR valve to be optimised within the constraints of an existing passive landing gear. The device was designed to be optimal in terms of its impact performance, which was demonstrated using numerical simulations of the complete landing gear system. To perform the simulations, assumptions were made regarding some of the parameters used in the MR shock strut model. In particular, the MR fluid's yield stress, viscosity, and bulk modulus properties were not known accurately. Therefore, the present contribution aims to validate these parameters experimentally, via the manufacture and testing of an MR shock strut. The gas exponent, which is used to model the shock strut's non-linear stiffness, is also investigated. In general, it is shown that MR fluid property data at high shear rates is required in order to accurately predict performance prior to device manufacture. Furthermore, the study illustrates how fluid compressibility can have a significant influence on the device time constant, and hence potential control strategies.

KEYWORDS: Magnetorheological, aircraft landing gear, semi-active damping, smart fluids, model validation.

* Corresponding author. Email: n.sims@sheffield.ac.uk; Tel: +44 (0)114 2227724.

1 INTRODUCTION

Smart fluids could be utilised to improve the performance of aircraft landing gears, which are subject to wide-ranging excitation conditions with conflicting damping requirements [1-4]. To demonstrate the feasibility of this solution, the smart device must adhere to stringent packaging constraints, which is an issue that researchers have often overlooked. The present authors considered packaging constraints in Part 1, where a methodology for optimising the impact performance of magnetorheological (MR) landing gears was detailed. In that study, the design methodology was demonstrated by sizing an MR valve for an existing commercial landing gear. Using an equivalent MR model of the existing system, it was shown that appropriate damping levels could be achieved for a wide range of impact conditions i.e. from the worst-case scenario, through to the least severe of impacts. However, the model format and its parameters were not validated experimentally. In particular, the MR fluid's yield stress, viscosity, and bulk modulus properties were not known accurately. The gas exponent, which is used to model the shock struts non-linear stiffness, must also be validated.

The aim of the present contribution is to experimentally validate the MR landing gear model developed in Part 1. This model was based upon that developed by Milwitzky and Cook [5] and so in this work, the authors will focus on validating the novel aspects of the revised model. These were: the inclusion of shocks strut fluid compressibility, the model of the MR flow behaviour, the magnetic design, and the device time constant. It transpires that these aspects of the model can be investigated by considering the MR shock strut independently from the rest of the landing gear structure, using various configurations of excitation velocity. As a result of this validation exercise, the model and design procedure described in Part 1 can be used to predict MR landing gear performance prior to device manufacture.

The present contribution is organised as follows. First, the design and manufacture of the MR landing gear shock strut is described. Next, the dynamic model of the shock strut is detailed. After describing the experimental facility, an investigation is presented which aims to validate the quasi-steady performance of the MR valve. Here, the accuracy of the yield stress and viscosity predictions is investigated. In a dynamic analysis, the aim is then to predict the sinusoidal response of the shock strut. This requires validating the MR fluid's bulk modulus and the gas spring function. Furthermore, an analysis of the device's time constant is given, which is a vital performance indicator when considering potential control strategies. After a discussion of the main results, conclusions are drawn and the requirements for further work are presented.

2 DESIGN AND MANUFACTURE OF THE MR SHOCK STRUT

In order to fabricate an MR landing gear shock strut for this investigation, it was decided to retrofit an MR valve to an existing passive device. In Part 1 an MR valve was optimised for the Polish Institute of Aviation's I-23 aircraft [6], which transpired to be a three-stage design. For the present study, it was not possible to obtain an identical I-23 shock strut to perform the validation. A full scale I-23 device would also have been oversized for the test facility used in this study. Consequently, the intention of this study was to build a more suitable lab scale device, which was achieved with a single stage design. The candidate shock strut was acquired from a RALLYE, which is a lightweight trainer/tourer aircraft built by the Socata company some years ago [7]. The numerical design tools outlined in Part 1 are directly applicable to this device, and so it is suitable for validation purposes. A schematic drawing of the RALLYE shock strut is shown in Figure 1(a).

In order to retrofit an MR valve, some design modifications were necessary and these are illustrated in Figure 1(b). As shown, the MR valve is incorporated within the inner cylinder, and the gas transfer tube has been removed, as this posed significant restrictions on the magnetic circuit. The MR valve is secured into place by the piston head, which completely seals against the outer cylinder. Therefore to prevent the formation of a vacuum, four fluid transfer orifices were included within the piston rod, which were sufficiently large that the pressure drop across them was negligible. Furthermore, to accurately characterise the performance of the MR valve, two pressure transducers [8] were incorporated, which were capable of reading both static and dynamic pressure. These were rated at 0-21MPa gauge and measured the fluid pressure on the 'non-gas side' of the piston, and the gas pressure on the 'gas side' (see Figure 1(b)). The shock strut was filled with AD57 MR fluid [9], and charged with Nitrogen gas to a pressure of 0.75MPa (at full extension of the shock strut).

The geometry of the MR valve was determined using the magnetic circuit sizing methodology developed in Part 1 by using a valve gap size equal to 0.6mm. The optimal design had three stages although, as mentioned earlier, only a single stage was manufactured. With reference to Figure 2, the resulting valve geometry and performance indicators of this single stage are given in Table 1. Where applicable, the performance was calculated by assuming a piston velocity of $1ms^{-1}$, which corresponded to the limitation of the experimental facility (Section 4). For the given constraints, this valve provided the greatest control ratio, and could achieve the maximum fluid yield stress without magnetic saturation, and without exceeding the maximum current rating of the copper wire. The method of assembly and manufacture of this valve is detailed in Figure 3. As shown, the annular valve gap was accurately maintained using two valve gap support spiders. These spiders were manufactured from titanium, whose non-magnetic properties direct the magnetic flux into the active region of the valve. The flux return and valve core were manufactured from a low-carbon mild steel due to its high

magnetic permeability. To wind the coil, small passageways were drilled into the valve core in order to provide exit routes for the wire. The coil was also surrounded with a wear resistant resin that was machined to the same diameter as the bobbin flange. This protected the coil from the abrasion of iron particles and furthermore, provided a smooth surface to encourage laminar valve flow. The wire was then routed outside through a separate port on the gas side of the device (see Figure 1(b)) and sealed with resin.

3 DYNAMIC MODEL OF THE MR SHOCK STRUT

In what follows, a model of the MR shock strut is detailed. This model was used in Part 1 in order to implement the design methodology, and to predict landing gear impact performance. In this discussion, attention will be drawn to the parameters that were assumed in Part 1, and which therefore require validation.

With reference to Figure 4, and neglecting internal friction forces, the total shock strut force F_s can be derived as:

$$F_s = (P_2 - P_1)a_{2i} + P_1 a_{1o} \tag{1}$$

where P_1 and P_2 are the pressures in chambers '1' and '2' respectively, a_{2i} is the inner cross-sectional area of the inner cylinder (or piston area) and a_{1o} is the outer cross-sectional area of the piston rod. The present study has assumed that the pressure in chamber '1' is equal to the gas pressure in chamber 'a'. This is valid when the fluid inertia is negligible and if the mass of the dividing piston is small. For the shock strut in this study, the fluid and gas volumes are mixed (i.e dividing piston mass = 0kg) and fluid inertia has been neglected for simplification purposes.

The gas pressure P_a (hence chamber '1' fluid pressure) is determined from the polytropic law for the compression of gases:

$$P_a (= P_1) = P_{a0} \left(\frac{v_{a0}}{v_a} \right)^m \tag{2}$$

where P_{a0} is the initial gas inflation pressure, v_{a0} is the initial gas volume, v_a is the current gas volume, and m is the polytropic exponent. In Part 1, m was assumed as 1.1, which has been shown to correlate well with observed behaviour when the fluid and gas volumes are mixed [10]. The term v_{a0} was determined as 60cm^3 by comparing the volume of MR fluid with the chamber volumes of the shock strut.

Assuming constant density, it can be shown that the general mass flow continuity equation accounting for the fluid compressibility of a control volume is given by:

$$\frac{dv}{dt} + \frac{v}{\beta} \frac{dP}{dt} = Q_i - Q_o \tag{3}$$

where v is the control volume (which changes according to piston position and/or fluid compression), β is the bulk modulus, P is the pressure and $Q_{i,}$ and Q_o are the volume flow rates into and out of the control volume respectively. In this equation, the bulk modulus β is unknown, and in Part 1, the base value for a standard hydraulic oil (β = 1.7GPa) was assumed as a reasonable approximation.

With reference to Figure 4, Eq.3 is applied to each fluid chamber, and essentially introduces non-linear stiffness terms to the model. During compression, $Q_{i2} = Q_{o1} = 0$, where subscripts '*1*' and '*2*' denote chambers *1* and *2*, respectively. Also, assuming there is no compression in the valve $Q_{o2} = Q_{i1} = Q$. Finally, assuming constant bulk modulus, the mass flow continuity equations for each chamber are:

$$Q = \frac{dv_1}{dt} + \frac{v_1}{\beta} \frac{dP_1}{dt} \tag{4}$$

$$-Q = \frac{dv_2}{dt} + \frac{v_2}{\beta}\frac{dP_2}{dt} \tag{5}$$

where $v_1 = v_{10} + v_{a0} + (a_{2i} - a_{1o})x - v_a$ and $v_2 = v_{20} - a_{2i}x$. Note that subscript '0' represents the initial conditions. Equations 1-5 were formulated in Simulink and the corresponding block diagram is shown in Figure 5. Here, Eq.4 is solved for v_1, whilst Eq.5 is solved for P_2. The gas volume v_a is then deduced by geometry, which in turn gives $P_a = P_1$ (Eq.2). Finally, in order to model the MR effect, a lookup table containing the pressure-flowrate (ΔP-Q) characteristics of the MR valve as a function of yield stress is generated. ΔP is calculated by summing the pressure drops across the active and inactive regions of the valve. The active pressure drop is determined by the solution of the Buckingham equation for Bingham plastic flow between parallel flat plates [11]. This has been shown to characterise smart fluids well for annular flow, where the height of the valve gap is negligible in relation to the mean valve diameter. The corresponding Buckingham equation is as follows:

$$4\left(\frac{l_a}{h\Delta P_{l_a}}\right)^3 \tau_y^3 - 3\left(\frac{l_a}{h\Delta P_{l_a}}\right)\tau_y + \left(1 - \frac{12\mu l_a Q}{bh^3 \Delta P_{l_a}}\right) = 0 \tag{6}$$

Here, ΔP_{l_a} is the active valve pressure drop, l_a is the active valve length (equal to $2t_b$ in Figure 2), b is the mean annular circumference of the valve (equal to $2\pi d$ in Figure 2), τ_y is the Bingham plastic yield stress, and μ is the viscosity of the MR fluid. The inactive pressure drop is readily determined using the equation for Newtonian flow between parallel flat plates, i.e. Eq. 6 with $\tau_y = 0$.

The two key unknowns in Eq. 6 are the MR fluid viscosity μ, and the Bingham plastic yield stress τ_y. As described in Part 1, the viscosity for AD57 MR fluid [9] was assumed as 0.1Pas. This value was estimated from relatively low shear rate data at 25°C, which was provided by

the fluid manufacturer. More specifically, the viscosity was an extrapolated value taken at the high shear rates anticipated within this flow mode MR landing gear. The yield stress was estimated using the fluid manufacturer's shear stress data, which was measured at a low shear rate of $1s^{-1}$, and 25°C. It is worth pointing out that these parameters are likely to be a function of temperature, and so the very low temperatures during aircraft flight may have an effect on the assumed values. Nonetheless, the assumptions are valid for the purpose of laboratory validation at room temperature, and if the present model can be validated, then viscosity and yield stress data obtained at different temperatures could be used with good credence.

A final important point is that the pressures in the dynamic shock strut model were found to drift when subject to several excitation cycles. This problem was also described by Patten, *el al*. [12], and occurs because of the constant density assumption in Eq.3. Nonetheless, the model was found to be accurate over a single cycle, particularly during the compression phase, which is the most important for landing impacts.

4 EXPERIMENTAL FACILITY

A schematic diagram of the experimental facility is shown in Figure 6, which illustrates the interaction between the various hardware and software components. To excite the MR landing gear shock strut, an Instron servo-hydraulic actuator and controller was used [13]. A Kepco BOP amplifier [14] also provided high bandwidth dynamic current control for the MR valve.

The hydraulic actuator was capable of delivering ±25kN force, ±50mm displacement and velocities of up to $\pm 1ms^{-1}$. As shown in Figure 6, the actuator position and current were controlled externally using real-time control software. Here, a host PC running xPC target [15] was used to develop the excitation signals and test automation scripts. This was coded in

Simulink, compiled as a C-programme, and subsequently downloaded onto a target PC, which performs the real-time control of the actuator. The data acquisition was achieved via a National Instruments data acquisition card [16], which could provide sample rates in excess of 10kHz. Once a test had completed, the measurement data was uploaded onto the host PC for post-processing. This measurement data was acquired from an inductive displacement transducer, which was also used for position feedback control of the actuator, and two pressure transducers (as described in section 2). Copper tubing was coiled around the shock strut body for cooling purposes. The tubing was fed with mains water, and allowed continuous testing without overheating of the shock strut.

5 QUASI-STEADY ANALYSIS

In what follows, an analysis is presented that aims to validate the quasi-steady pressure/flowrate function of the MR valve i.e the Buckingham equation (Eq. 6). The validated function can then be used as a lookup table within the shock strut model to predict the dynamic behaviour.

The experimental quasi-steady behaviour was determined using a constant velocity excitation, where the aim was to achieve a steady-state pressure drop. This was applied only in the compression phase of the shock strut's stroke. The extension phase was not considered, as the initial shock strut pressure was not high enough to prevent cavitation of the fluid. The valve pressure drop was then calculated by subtracting the pressure sensor readings. Here, it is assumed that the gas pressure is equal to the fluid pressure in the piston rod, which is a valid assumption as there is no dividing piston.

A typical result from this test is shown in Figure 7. This is shown for a step-velocity excitation between $0ms^{-1}$ to $0.1ms^{-1}$, and for a range of input currents between 0A and 2A.

Clearly, steady-state conditions are soon achieved after the step velocity change is applied. The quasi-steady pressure drop can therefore be determined, which was calculated as the mean value over the second half of the response. This was repeated for velocity excitations between $0.01ms^{-1}$ and $0.4ms^{-1}$ in order to form the quasi-steady valve function.

Before the numerical model can be correlated with experimental data, the yield stress/current relationship of the MR valve must be determined. This was calculated by performing a 2-D axisymmetric finite element analysis (FEA) of the MR valve, which was carried out using FEMM software [17]. FEA was used instead of the more straightforward analytical analysis presented in Part 1, as it permitted the effects of flux leakage to be more accurately accounted for. In this analysis, the mean flux density across the active valve length was calculated for each current magnitude. The yield stress corresponding to this mean applied field was then determined using the fluid manufacturer's data. Consequently, the Buckingham equation can be formulated and compared to the experimental quasi-steady valve performance.

The corresponding results are shown in Figure 8 for the 0A and 1A responses. In the initial model, a viscosity equal to 0.1Pas has been assumed (as described in Section 3). Also, the initial yield stress values are 0kPa for the 0A response, and 16kPa for the 1A response (from FEA). Clearly, the numerical results do not correlate well with the experimental behaviour, since the viscosity and yield stress predictions are too low.

To improve correlation, these parameters were updated, and the corresponding results are also shown in Figure 8. Here, the viscosity was increased to 0.14Pas, and the yield stress for the 1A response was increased to 43kPa. As shown, these updated values significantly improve the model's prediction of the low velocity behaviour. However, correlation deteriorates at high velocities, where the experimental response is more quadratic in nature. This could be attributed to a shear-thickening phenomenon [18], where the apparent viscosity increases with

increasing shear rate. The Buckingham equation, which uses the Bingham plastic relationship between shear stress and shear rate, does not account for such behaviour. Another explanation could be due to minor losses or turbulence effects, which are a function of the velocity squared. The flow within the valve was expected to be laminar (*Re* in Table 1 is less than 1000) but minor losses could have been induced around the valve gap support spiders that partially obstruct flow (see Figure 3). Changes in temperature may also have affected the viscosity. For example, the fluid manufacturer's viscosity information was measured at 25°C. However, the actual fluid temperature may have been lower than this due to the presence of the cooling circuit.

To summarise the yield stress results, Figure 9(a) compares numerical predictions (calculated indirectly from FEA) with the experimentally identified values between 0A and 2A. Two data sets are shown for the yield stress predictions – one used the original fluid magnetic flux density/magnetic field strength measurements (B_f-H_f) in the FEA analysis (i.e. those used to design the valve and to plot the 'initial model' responses in Figure 8), and the other used an updated B_f-H_f curve that was calculated using a different method. The corresponding mean values of flux density in the valve gap (calculated directly from FEA) are also given in Figure 9(b). It is apparent that the original error in the yield stress predictions was partly due to inaccurate B_f-H_f data, which meant that the magnetic flux density (Figure 9(b)) and hence yield stress (Figure 9(a)) in the valve gap was underestimated. The updated B_f-H_f curve provides a significant improvement in correlation with the experiment, particularly for low current values. At higher currents, the yield stress is still underestimated by up to 23% of the experimental value. However, the largest experimental value is in fact 18% greater than the maximum yield stress specified for the AD57 MR fluid, which is 55kPa at 0.7T [9]. This could be explained by a variation in fluid properties between batches, or even due to an

inhomogeneous volume fraction of iron particles. For example, the MR fluid was observed to be fairly susceptible to sedimentation problems.

6 DYNAMIC ANALYSIS

In the following analysis, the aim is to accurately predict the dynamic response of the shock strut. First, the bulk modulus of the MR fluid, and the shock struts gas spring function are validated. The validated parameters and the updated quasi-steady valve function (from Section 5) are then used to predict the sinusoidal response of the shock strut. Finally, an investigation is presented to identify the time constant, which is an important performance indicator when considering potential control strategies.

6.1 Fluid compressibility

The compressibility of a fluid directly determines the rate of change in fluid pressure. An effective way to investigate this, and hence validate the associated bulk modulus β, is to analyse the pressure transients in a step-velocity test. Here, an incompressible fluid would correspond to an instantaneous development of the quasi-steady valve pressure drop.

The results from this analysis are shown in Figure 10 for a step velocity input between 0ms^{-1} and 0.1ms^{-1}, and for current excitations of 0.5A and 1A. The updated quasi-steady valve function has been included in the model, which is accurate for the chosen input conditions (see Figure 8). As indicated by the steep pressure gradients, the numerical response with β = 1.7GPa is too ‘stiff’. By updating the bulk modulus to 0.3GPa, i.e. to a more compressible (or less stiff) value, the correlation in slope with the experiment is improved. However, the model does not account for the higher order dynamics observed in the experiment. For example, the rate of change in pressure in the experiment is more gradual at the beginning than at the end of the response. Furthermore, the experimental response has an

'underdamped' nature. This could be attributed to fluid inertia, which is not accounted for in the model. Nonetheless, the general slope of the experimental response correlates well with the model, and thus serves as a useful methodology to approximate the bulk modulus of the MR fluid. The lower observed value of 0.3GPa is probably due to entrapped air, which will have been introduced during mixing of the fluid prior to filling.

6.2 Gas model

Before the dynamic response of the shock strut model can be investigated, the gas law (see Eq. 2) must first be validated. The key parameters that require validation are the initial gas volume v_{a0} and the gas exponent m.

As mentioned in Section 3, the initial gas volume was calculated as 60cm^3. However, due to filling difficulties, a degree of error is probable in this calculation. Consequently, v_{a0} must be validated, and this was effectively achieved using the following isothermal analysis. In the experiment, pressure measurements were taken in 2mm increments across the full stroke of the shock strut. Between each measurement, enough time was allowed to ensure that the pressure had reached a steady isothermal value. The experimental results are shown in Figure 11(a) as the 'stationary measurements'. The results are then compared to a simulation of the gas pressure in the dynamic model with m = 1 i.e. an isothermal compression, and with β = 0.3GPa (the updated value). Also, the initial gas pressure (P_{a0}) was determined according to the experimental reading. As shown in Figure 11(a), by updating the initial gas volume from 60cm^3 to 66cm^3, excellent correlation in the isothermal gas pressure is achieved.

Identification of the gas exponent is addressed in Figure 11(b). Here, the numerical and experimental gas pressure responses are compared using sinusoidal excitations. As shown, by updating the gas exponent from m = 1 to m = 1.33, good correlation is achieved. This

suggests that the gas compression is more adiabatic than expected, where m = 1.1 was originally assumed (Section 3). The reason for this could be explained by considering the difference in flow regimes between passive and MR shock struts. For example, the assumed value was based on typical behaviour from conventional passive shock struts [10], which rely upon turbulent flow. In contrast, MR damping is based upon laminar flow. Therefore, in the passive shock strut, more energy is likely to be transferred away from the gas as a result of the more vigorous/turbulent mixing with the fluid. Consequently, the gas exponent will be more isothermal in nature. Further credence is given to this point by considering a passive device that uses a floating piston to separate the fluid and gas. Currey [10] suggests that the more adiabatic value of m = 1.35 should be used, which correlates well with the observed MR behaviour.

A final point is how the model does not account for the observed hysteresis in the experimental response. This is attributed to the heat transfer processes within the shock strut, which is associated with a variable gas exponent m. Wahi [19] demonstrated how this could be modelled in landing gear. However, for the purpose of the present study, the accuracy obtained with the existing model was considered as acceptable (Figure 11(b)).

6.3 Prediction of the sinusoidal response

In this section, the updated quasi-steady valve function (Section 5), bulk modulus (Section 6.1), and gas law (Section 6.2) are used to validate the dynamic behaviour of the shock strut model. This is investigated using two types of sinusoidal excitation. First, complete cycles were used to validate the low velocity behaviour. Here, the velocity and current was limited in order to prevent fluid cavitation during the extension phase of the stroke. Therefore, to investigate higher velocity/higher current behaviour, half cycles were applied in the

compression phase only. In the analysis, shock strut pressures are modelled rather than force. This enables the effects of friction to be eliminated, which were found to be fairly significant.

Figure 12 compares the model predictions with experiment, for a full sinusoidal excitation with amplitude a = 25mm, and frequency f = 0.5Hz. Here, the fluid pressure on the non-gas side of the piston (P_2 in Figure 4) is shown as a function of displacement. Displacement is used because it provides a better insight to the gas spring effect, which contributes significantly to the response (due to the large stroke). Clearly, correlation is excellent throughout the range of excitation currents.

As a further example, Figure 13 presents the results for a full sinusoidal excitation with a = 10mm, and f = 0.5Hz. This time, the fluid pressure is shown as a function of velocity, which is more appropriate as the damping effect dominates the response. Again, excellent correlation is observed, particular in the post-yield behaviour. The fluid compressibility effect can be observed through the hysteresis in the pre-yield behaviour. The observed inaccuracies in this region may be attributed to the un-modelled higher order dynamics (see Figure 10). Nonetheless, correlation is still good.

Higher velocities are investigated in Figure 14 using a half cycle with a = 25mm, and f = 3Hz. Rather than plotting the fluid pressure on the non-gas side (as in Figures 12 and 13), the pressure difference across the valve has been plotted as a function of piston velocity. This is to isolate the gas spring effect, thus providing a better insight of the device's damping behaviour. As expected, the model breaks down at higher velocities due to the quadratic damping effect in the experimental response.

6.4 Device time constant

The time constant is a vital performance indicator and will have a large influence on potential control strategies. The power supply, the magnetic circuit design, and the smart fluid rheology all contribute to the time constant associated with a change in the excitation current. Furthermore, fluid compressibility will have an affect, and must be isolated from the other contributors.

In the present study, the time constant was investigated by applying a step change in current, from I_1 to I_2, during a constant velocity excitation. This step change was generated by using the amplifier in current control mode. The corresponding yield-stress response in the dynamic shock strut model was then simulated using the following transfer function G.

$$G(s) = \frac{1}{\tau s + 1} \tag{7}$$

Here, τ is the time constant, and s is the Laplace operator. To identify the time constant, the transient behaviour between the steady-state pressure levels can be correlated. The numerical and experimental step responses are shown in Figure 15 for I_2 = 1A and I_2 = 2A. The initial current for both cases corresponds to I_1 = 0.5A. In Figure 15, the 'ideal response' assumes that the step change in yield stress is generated instantaneously. This represents the effects of fluid compressibility only. Therefore, the observed error between the ideal case and the experiment corresponds to the time response of the power supply, magnetic circuit, and fluid rheology. As shown in Figure 15, the time constant associated with these factors was identified as τ = 1.8ms, where excellent correlation with the experiment is observed. Due to the use of a current driver in the experiment, this is approximately 76% lower than the predicted value given in Table 1, which was calculated by assuming a constant voltage

source. This rapid response suggests that the landing gear shock strut would be highly suitable as a basis for feedback control, particularly with current controlled power source.

The time constant of the complete response (i.e. including fluid compressibility effects) was also calculated as 2.5ms, which is the time taken for the pressure to reach 63% of its final value. Therefore, the overall time constant is increased by 28% due to compression of the fluid. This is likely to become even more significant at higher velocities, but could be improved via the removal of entrapped air prior to filling e.g. using a vacuum pump.

7 DISCUSSION

In the present study, it has been shown that an accurate model of the MR valve's quasi-steady performance will result in good predictions of the shock strut's dynamic behaviour. However, using the existing Buckingham equation for Bingham plastic flow, only the low velocity behaviour produced good agreement due to a quadratic damping effect. The Bingham plastic model could potentially be modified to better characterise the MR fluid's high velocity behaviour. For example, Lee and Wereley [18] showed how the Herschel-Bulkley model could be used to account for shear-thickening and shear-thinning phenomena in flow mode devices. Such methods could be adopted to further update the model and hence enhance predictions of high velocity behaviour. Another approach was developed by Peel and Bullough [11] who used a dimensionless form of the Buckingham equation, and showed how empirical relationships could be defined to describe shear-thinning behaviour. This dimensionless approach means that the updated model can be applied to design new devices i.e. the model represents the fluid behaviour and is not device specific. However, before applying such methods in the present study, the errors in the yield stress predictions and the quadratic damping effect must be formally understood. This will require more detailed

information about the MR fluid's yield stress and viscosity properties, and the degree of variation between batches. Furthermore, higher velocity shear stress/shear rate characteristics of the MR fluid are required. For example, fluid data for AD57 MR fluid is available at shear rates up to $1000s^{-1}$ [9]. However, in the flow mode shock strut, shear rates were found to be two orders of magnitude greater than this. If in fact it transpired that the quadratic damping effect was a result of minor losses rather than shear thickening, the model could be updated accordingly. However such effects will be device specific and could be minimised by changing the valve design or method of assembly.

In Part 1, it was suggested that turbulence could hinder device performance as a result of the large impact velocities associated with landing gear. Perhaps there is evidence of this in the present study if the quadratic damping effect is indeed due to turbulence. For example, through observation of Figure 8 and Figure 14, it can be seen how the difference between the on and off-state pressure drop deteriorates due to the more substantial quadratic damping effect in the zero-field condition. It would be interesting to investigate performance at higher 'effective' Reynolds numbers. However, the test facility was limited to operating at relatively low sub-critical Reynolds numbers below 1000. Such behaviour could be investigated using impact tests in order to overcome the velocity limitations of the hydraulic actuator.

8 CONCLUSIONS

In this paper, the manufacture and testing of an MR oleo-pneumatic landing gear shock strut was described. This was sized and modelled using the numerical approach outlined in Part 1, where the aim was to validate the MR landing gear design methodology.

In a quasi-steady analysis, it was found that the original analytical predictions of yield stress and viscosity were poor. The analytical yield stress predictions were later improved when a

different magnetic characterisation for the MR fluid was used in the FEA analysis. After updating the model parameters, the prediction of the low velocity quasi-steady behaviour was good, but correlation at higher velocities deteriorated.

In a dynamic analysis, the bulk modulus of the MR fluid was identified as 0.3GPa. In general, this resulted in a good prediction of the pressure transients, but the model failed to account for higher order dynamics, and fluid inertia. The gas exponent was identified as 1.33, which is higher than the value commonly used for an equivalent passive shock strut. It was thought that this could be attributed to the differing valve flow regimes, and hence heat transfer characteristics between passive and MR devices. By then formulating the dynamic shock strut model with the updated parameters, excellent correlation with the experimental behaviour was demonstrated using low velocity sinusoidal excitations. Therefore, if an accurate model of the quasi-steady behaviour can be developed, a good prediction of the dynamic shock strut performance will result.

However, in order to validate the landing gear design methodology, the quasi-steady MR valve function must be formulated analytically, without the need to update the yield stress and viscosity parameters. It has been shown that the prediction of yield stress is highly dependant on obtaining accurate magnetic fluid property information. Furthermore the prediction of viscosity was inaccurate due to a quadratic damping effect, which is not yet formally understood. This will be dependant on acquiring more detailed fluid property information at significantly higher shear rates. It was also thought that fluid batch variations and sedimentation could have influenced the results. Preventing sedimentation will be vital for landing gear applications due to the highly intermittent nature of the input excitation.

The present study has focused on the relatively low velocity behaviour of MR landing gear shock struts. Future work should investigate the performance at higher velocities using

impact tests. This will permit a more detailed assessment of valve turbulence, fluid compressibility and hence controllability. Fluid compressibility is likely to be particularly important at higher velocities, where it was found that at just $0.1ms^{-1}$, the time constant was increased by 28%.

9 REFERENCES

1. ADLAND, *Adaptive landing gears for improved impact absorption*. 2005, Project reference number: IST-FP6-2002-Aero-1-502793-STREP, http://smart.ippt.gov.pl/adland/,
2. Berg, C D and Wellstead, P E (1998), "The application of a smart landing gear oleo incorporating electrorheological fluid", *Journal of Intelligent Material Systems and Structures*, **9**(8), 592-600.
3. Choi, Y T and Wereley, N M (2003), "Vibration control of a landing gear system featuring electrorheological/magnetorheological fluids", *Journal of Aircraft*, **40**(3), 432-439.
4. Ervin, R D, Lou, Z, Filisko, F E, and Winkler, C B (1996), "Electrorheology for Smart Landing Gear", *NASA-CR*, **200883**.
5. Milwitzky, B and Cook, F E (1952), "Analysis of landing-gear behavior", *NACA Report*, **1154**.
6. Institute of Aviation, http://www.ilot.edu.pl/, Al. Krakowska 110/114, 02-256 Warszawa, Poland.
7. Socata (2005), http://www.socata.org/.
8. RDP Electronics Ltd (2005), Grove Street, Heath Town, Wolverhampton, WV10 0PY, United Kingdom, http://www.rdpe.com.
9. Fraunhofer Institut Silicatforschung (2005), http://www.isc.fraunhofer.de/.
10. Currey, N S (1988), *"Aircraft Landing Gear Design: Principles and Practices"*, American Institute of Aeronautics and Astronautics, Inc.
11. Peel, D J and Bullough, W A (1994), "Prediction of ER valve performance in steady flow", *Proceedings of IMechE Part C: Journal of Mechanical Engineering Science*, **208**, 253-266.
12. Patten, W N, Mo, C, Kuehn, J, and Lee, J (1998), "A primer on design of semiactive vibration absorbers (SAVA)", *Journal of Engineering Mechanics - ASCE*, **124**(1), 61-68.
13. Instron Structural Testing Systems. 2004, http://www.instron.com, IST GmbH, Landwehrstrasse 65, 64293, Darmstadt, Germany.
14. Kepco Inc. 2004, www.kepcopower.com/bop.htm, 131-138 Sanford Avenue, Flushing, NY 11352 USA.
15. xPC Target. 2002, The MathWorks, Inc., 3 Apple Hill Drive, Natick, MA,
16. National Instruments. 2002, www.ni.com, 11500 N Mopac Expwy Austin, TX 78759-3504.
17. FEMM. 2005, Foster-Miller, Inc., 350 Second Avenue, Waltham, MA 02451, USA, http://femm.foster-miller.net/index.html,
18. Lee, D-Y and Wereley, N M (1999), "Quasi-steady Herschel-Bulkley analysis of electro- and magneto-rheological flow mode dampers", *Journal of Intelligent Material Systems and Structures*, **10**, 761-769.
19. Wahi, M K (1976), "Oil compressibility and polytropic air compression analysis for oleopneumatic shock struts", *Journal of Aircraft*, **13**(7), 527-530.

ACKNOWLEDGEMENTS

The authors are grateful for the support of the European Commission under project reference No. FP6-502793 (The ADLAND project). The authors would also like to acknowledge the EPSRC for the studentship awarded to D.Batterbee.

	Parameter	Symbol/unit	Value
Geometry	Valve length	l /mm	14
	Number of valve stages	n	1
	Valve gap height	h /mm	0.6
	Bobbin core radius	t_a /mm	5.79
	Flange height	t_b /mm	2.89
	Mean valve diameter	d /mm	20.42
	Outside diameter	D /mm	28
	No. of turns of copper wire (Diameter = 0.45mm)	N/-	136
Performance	Dimensionless valve length	α/-	0.41
	Flux density in the steel at maximum yield stress	B_S /T	1.18
	Current to achieve $\tau_{y_{max}}$	I /A	2.39
	Power to achieve $\tau_{y_{max}}$	P/W	5.27
	Pressure drop at $\tau_{y_{max}}$ (piston velocity = 1ms^{-1})	ΔP_{max} /MPa	3.02
	Control ratio (piston velocity = 1ms^{-1})	λ/-	2.26
	Reynolds number (piston velocity = 1 ms^{-1})	Re/-	815
	Time constant	τ /ms	7.6

Table 1: Geometry and performance of the optimised valve. Values calculated using methods described in Part 1.

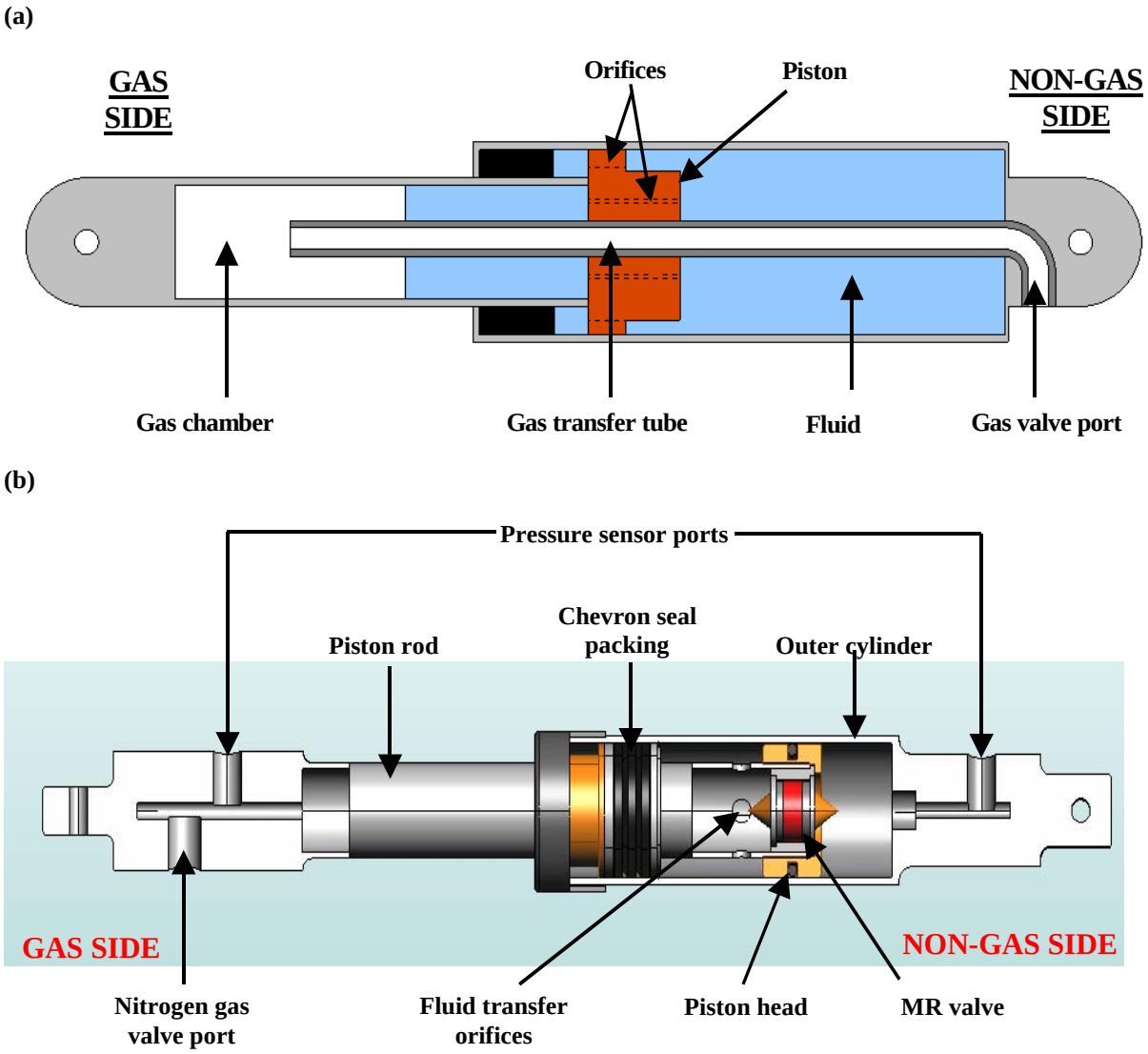

Figure 1: Schematic diagrams of the oleopneumatic shock struts. (a) Commercial passive shock strut taken from a RALLYE aircraft and (b) modified shock strut with MR valve.

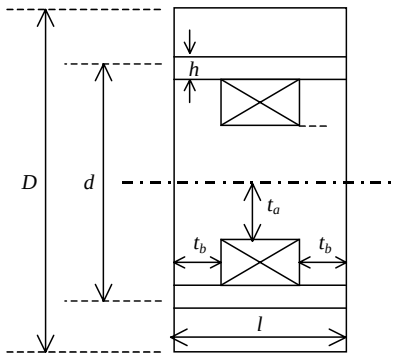

Figure 2: MR valve geometry nomenclature.

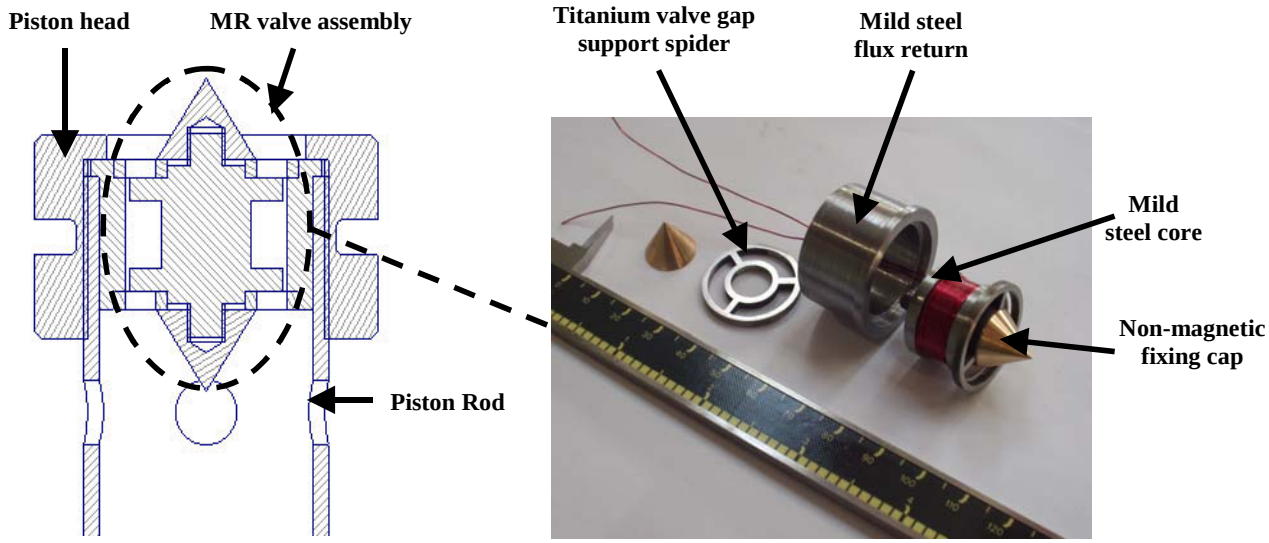

Figure 3: MR piston head design

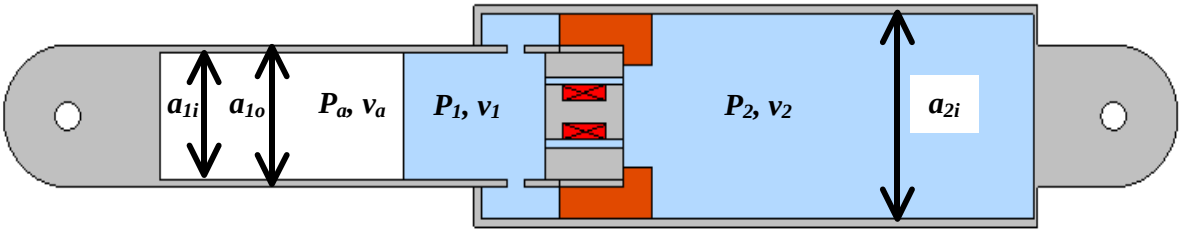

Figure 4: Schematic diagram of the MR shock strut

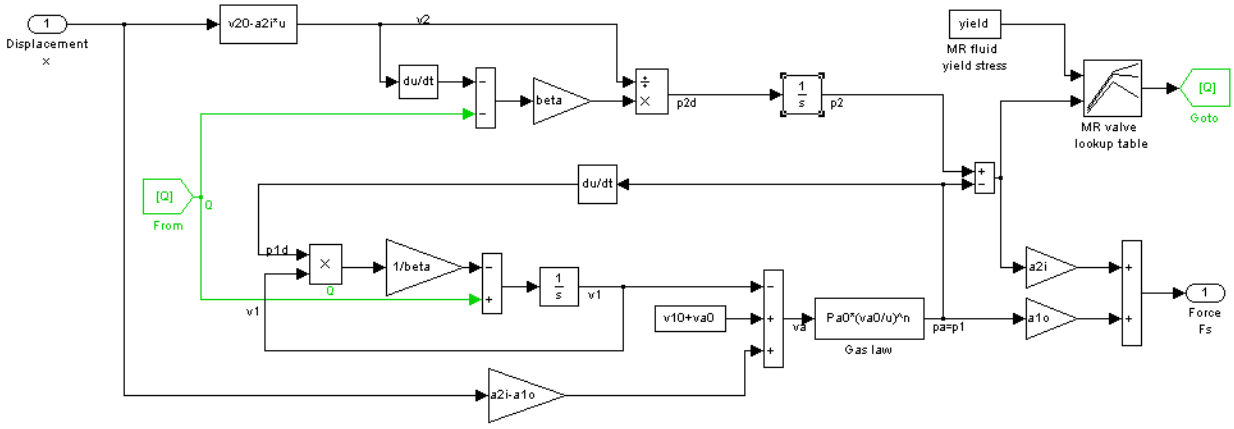

Figure 5: Simulink block diagram of the dynamic MR shock strut model.

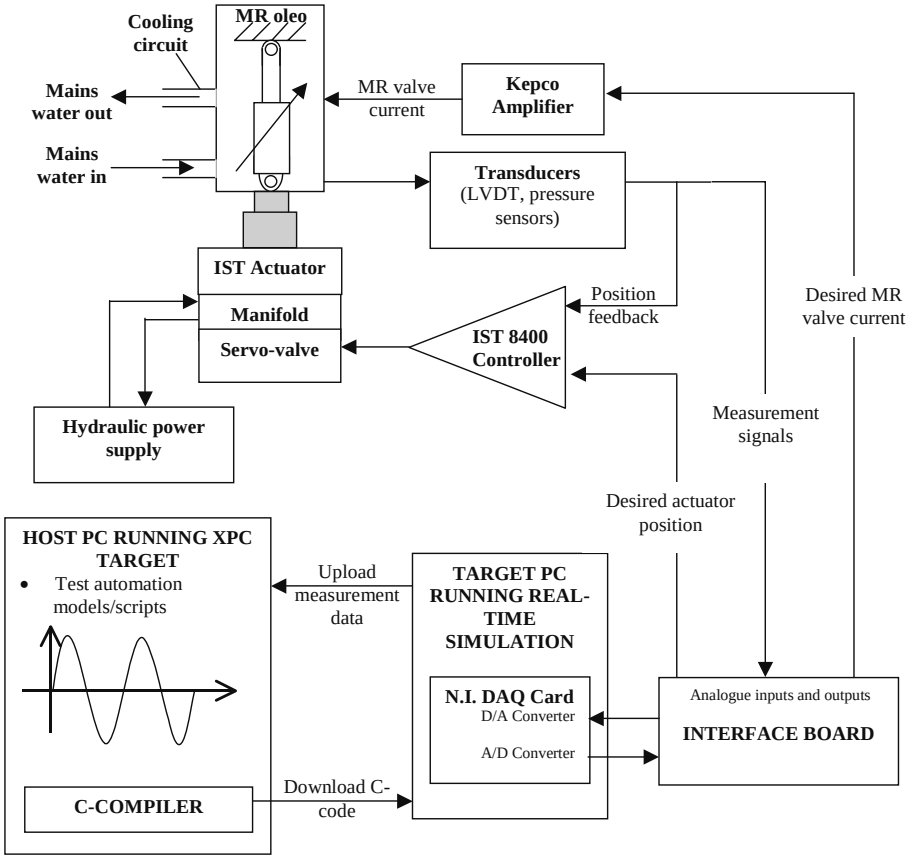

Figure 6: A schematic diagram of the experimental facility.

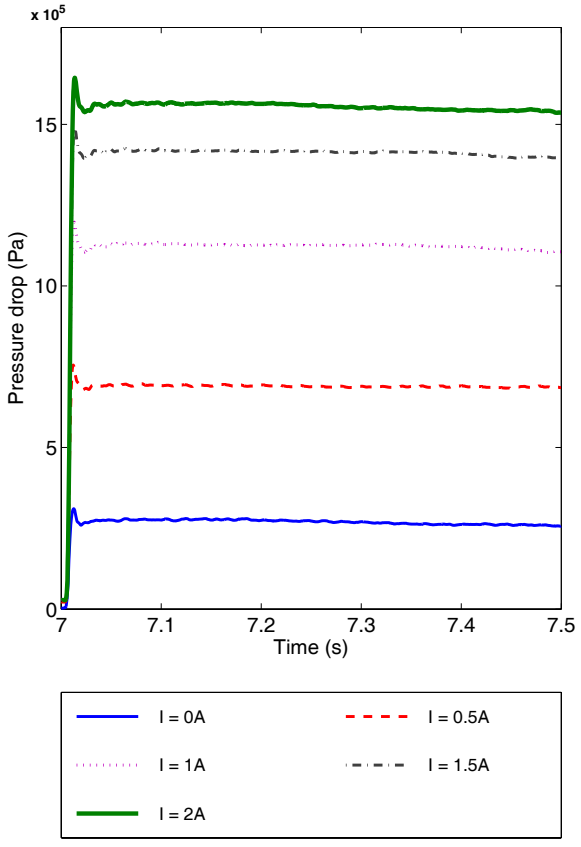

Figure 7: Quasi-steady pressure drop. V = 0.1ms^{-1}.

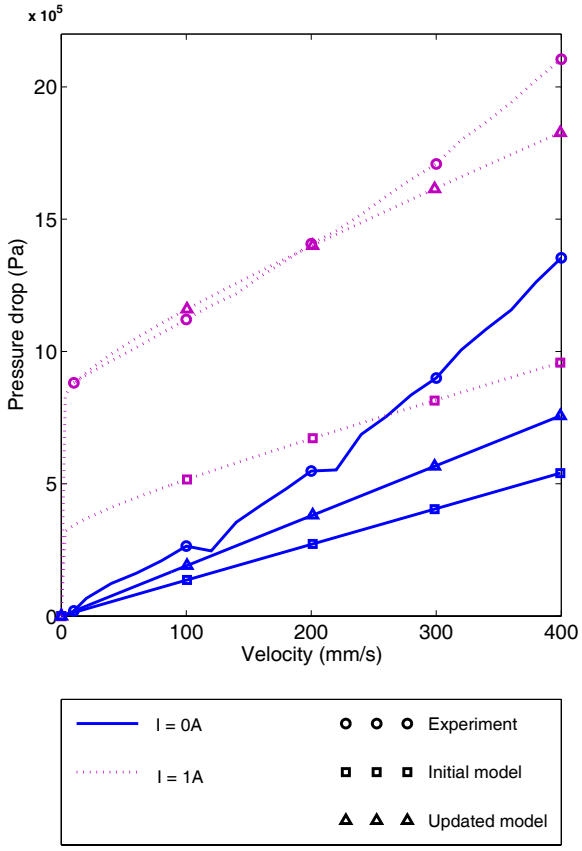

Figure 8: A comparison between the modelled and experimental quasi-steady pressure/velocity characteristics.

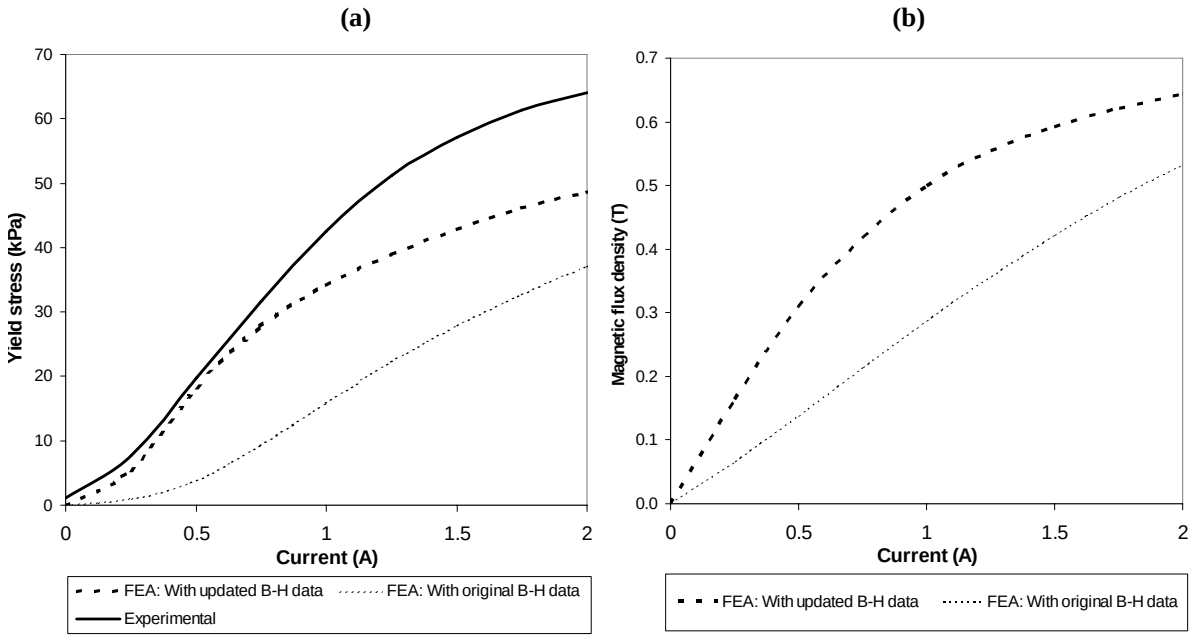

Figure 9: Results from the finite element magnetic circuit analysis. (a) Experimental and numerical yield stress/current curves and (b) the corresponding numerical magnetic flux density/current curves.

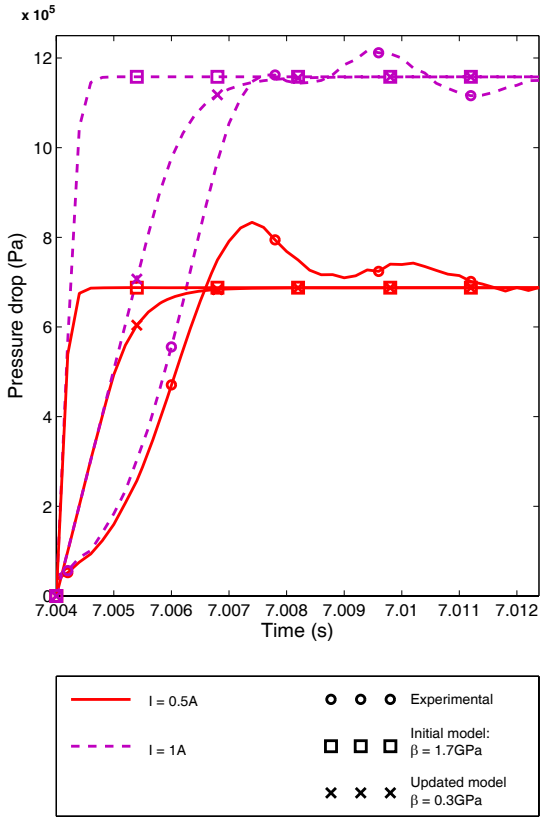

Figure 10: Identification of the MR fluid bulk modulus β using the pressure transients in a step-velocity test. Initial velocity = 0ms^{-1} and final velocity = 0.1ms^{-1}.

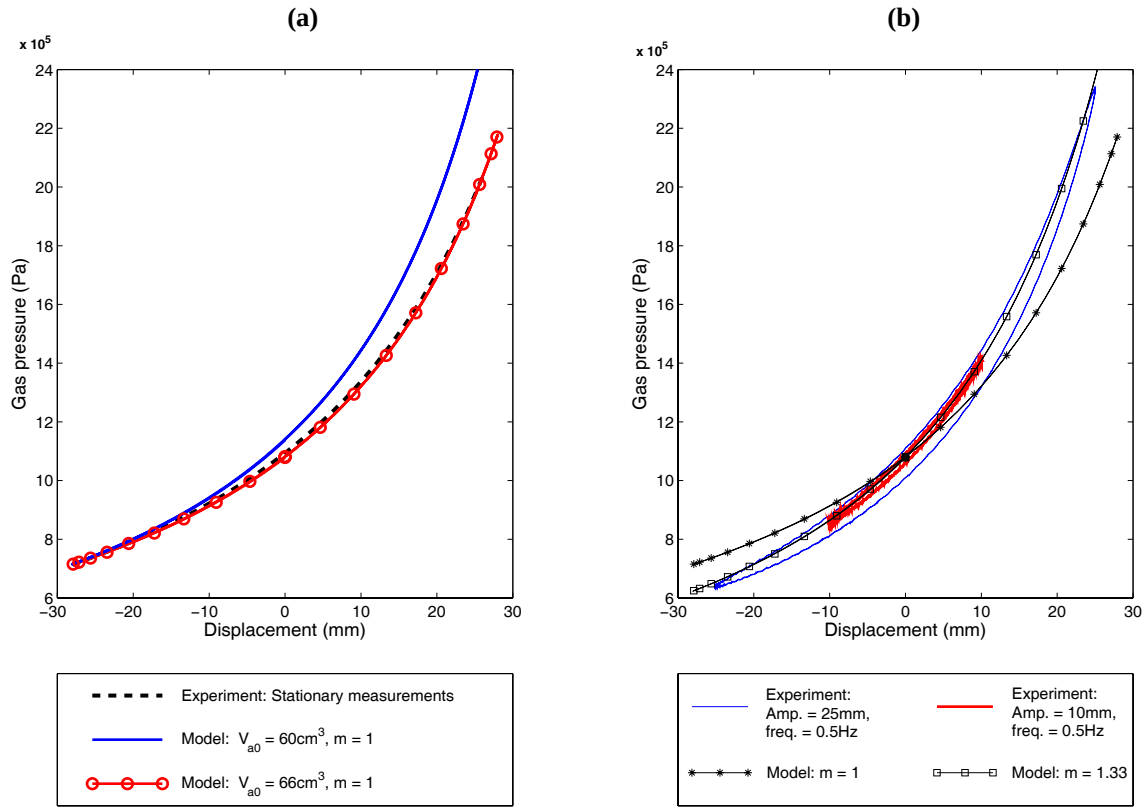

Figure 11: Identification of the gas model parameters. (a) Initial gas volume v_{a0} and (b) gas exponent m. β = 0.3GPa.

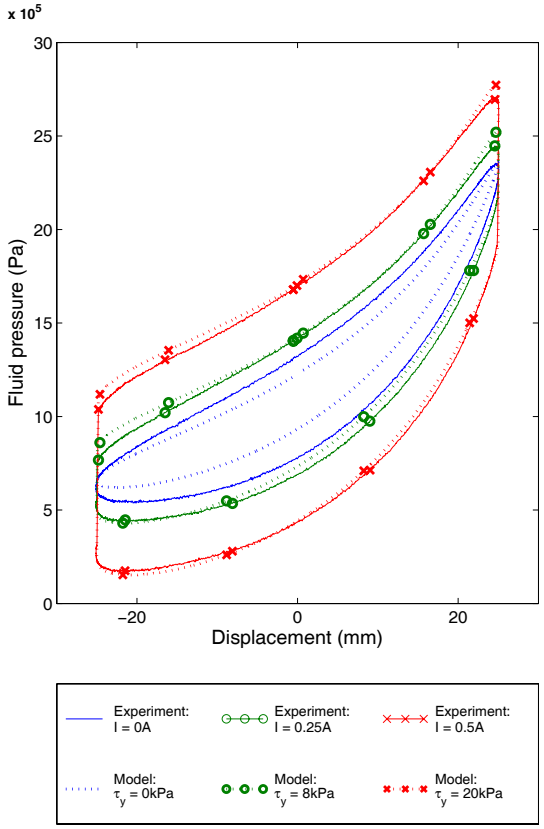

Figure 12: Simulated and experimental pressure (non-gas side)/displacement responses for a sinusoidal excitation. a = 25mm, f = 0.5Hz.

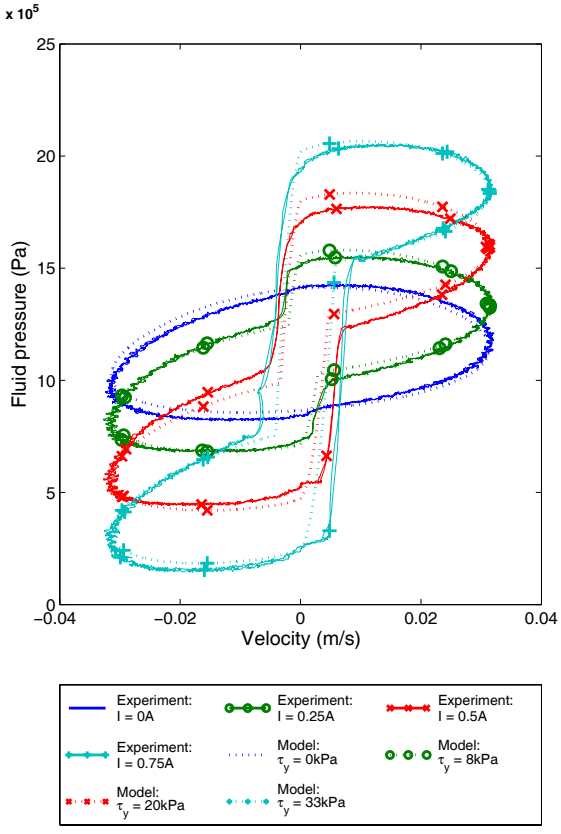

Figure 13: Simulated and experimental pressure (non-gas side)/velocity responses for a sinusoidal excitation. a = 10mm, f = 0.5Hz.

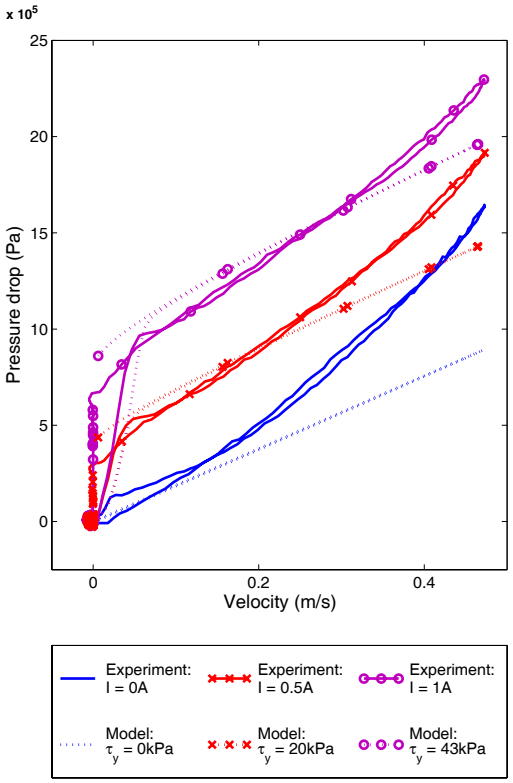

Figure 14: Simulated and experimental valve pressure drops during a half-sine test. a = 25mm, f = 3Hz.

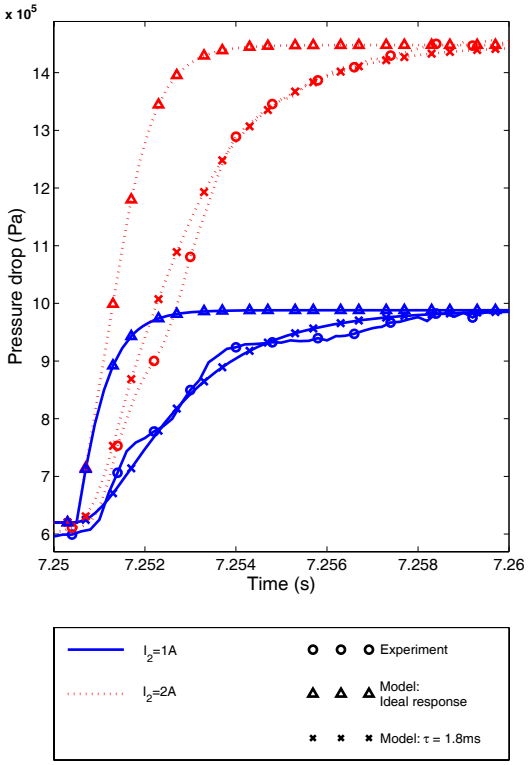

Figure 15: Prediction of the response to a step change in current. I_1 = 0.5A, V = 0.1m/s.